

Mapping erosion-corrosion of carbon steel in oil exploration conditions: some new approaches to characterizing mechanisms and synergies

M.M. Stack and G.H. Abdulrahman

Department of Mechanical Engineering
Strathclyde University

75 Montrose Street
Glasgow, G1 1XJ, UK

E-mail: margaret.stack@strath.ac.uk

Phone No: +441415483754

Fax No: +44 141 552 5105

Abstract

Erosion by solid particles in oil/water slurries is a technologically important area. In such conditions, it is necessary to distinguish between the effects of the sand, aqueous environment, and the oil. Erosion-corrosion maps provide a means of identification between erosion-corrosion regimes as a function of erosion and corrosion parameters. However, there has been no work carried out to map the effects of parameters in oil/water slurries. This paper investigates the effect of erosion-corrosion on carbon steel in oil field production and maps the results. Distinctions between "synergistic" and "additive" erosion-corrosion behaviour are superimposed on the maps in the various environments.

1. Introduction

Erosion-corrosion is a major issue in oil exploration, Figs. 1-2. In particular, in the exploration phase i.e. drilling in crude oil sand slurries, wear of the materials such as drilling tools and pipes may occur. In such cases, the degradation may be caused by a number of factors relating to the particles, pipe and drilling materials and the environment [1-3].

Although there have been a significant number of researches into the role of the aqueous environment in the synergy between erosion and corrosion of materials [4-10], there have been very few studies to investigate such effects in crude oil conditions. In particular, the separate effects of the sand slurry aqueous solution, the oil environment and the interactions of the latter processes together have not been considered. This is despite the application of such studies in oil exploration conditions.

Advances in the study of erosion-corrosion in recent years have led to the construction of erosion-corrosion mechanism maps [4-7]. This provides a means of assessing the transitions between the regimes as a function of the main process

parameters. However, to date there have been no such maps developed for application to erosion-corrosion in oil exploration conditions.

In this paper a study was conducted of the effects of erosion-corrosion of carbon steel in a range of conditions, reservoir water with sand, oil with sand and the combination of both conditions. Erosion-corrosion maps were constructed showing the extent of wastage, the mechanism of degradation and the synergism/antagonism between the processes as a function of impact angle and particle velocity. The advantages and limitations of such maps together with the potential applications are addressed in this paper.

2. Experimental details

2.1 Erosion-corrosion test methods

Erosion–corrosion tests were carried out using an impinging jet apparatus, as shown in Fig. 3 [11] and is described elsewhere [4,11]. This consisted of a jet of particles in an aqueous flow enabling the effect of erosion variables to be evaluated independently of each other. The impact angle of the specimen could be varied by rotating the specimen. The velocity was calibrated through knowledge of the geometry of the outlet jet.

The slurry consisted of silica sand of size range 600 -710 μm . The particle concentration in the slurry solution was 20% by volume.

The test specimen was connected to an electrochemical cell, as shown elsewhere [10]. The reference electrode was Saturated Calomel. Potentiodynamic polarization curves were measured through sweeping the potential in a positive direction from -800 to 800 mV at a sweep rate of 200 mV min^{-1} during the test. Erosion–corrosion tests were performed at three applied potentials of -400 mV, 0 mV and 400 mV for 30 minutes using a computer controlled ACM potentiostatic to fix the potential at the required value.

The test material was carbon steel (X52) supplied by Kelvin Steel Glasgow with chemical composition as percentage: 0.18, Mn 1.6, Si 0.55, Cr 0.25, Cu: 0.35, Ni: 0.3, S: 0.008. Three environments were evaluated, i.e. reservoir water (4M NaHCO₃ +NaCO₃ of pH 8.25), crude oil and 20% reservoir water with crude oil.

The chemical composition of crude oil in ppm (mass) was (Ca: 33.26, Na: 4.26, K: 1.07, H₂S: 0.0007). The specific gravity was 0.77 and density was 767 g l⁻¹.

The dimensions of the specimens were 25mm × 10mm × 4 mm. The area exposed to impingement jet was 0.19 cm², whilst the remaining area was covered by a coating in order to ensure that all corrosion measurements related to the erosion-corrosion process only. Mass change measurements were made of the samples post testing using a Mettler electronic balance. The tests were carried out at three impact angles i.e. 15°, 45° and 90° and three velocities i.e. 2.5, 3.5 and 4.5 ms⁻¹, for 30 minutes. The reproducibility of the experiments was estimated to be ± 5% calculated between two consecutive experiments.

At the end of the test, the samples were cleaned with distilled water to remove any deposited material. Following exposure, the morphology of the eroded specimens was evaluated using scanning electron microscopy (SEM).

3. Results

3.1 Potentiodynamic polarization results

Polarization curves, Fig. 4 (a), showed that following erosion-corrosion in the water environment at 15°, there was a general increase in anodic current density with increasing velocity from 2.5 to 4.5 ms⁻¹. Clear evidence of passivation was observed. The value of zero current potential shifted in a negative direction with increasing velocity. A similar pattern was observed for the carbon steel in the crude oil environment, Fig. 4(b), with anodic current density increasing with velocity. However, in this case, the current density was more than two orders of magnitude less than in the previous case. In the combined crude oil/ reservoir water environment, Fig. 4(c), similar behaviour was observed in terms of the passivation trends;

however, in this case, the anodic current densities were greater than those in the crude oil environment, Fig. 4(b), by an order of magnitude but less than in the water and oil environment, Fig. 4(c).

At higher impact angles, i.e. 45 °, Fig. 5(a-c), a generally similar variation with impact velocity was observed. However, in this case the anodic current densities were marginally higher than at the lower impact angles. At the highest impact angle studied, i.e. 90°, Fig. 6(a-c), the values of the anodic current densities appeared similar to those at 45°, Fig. 5(a-c).

It was interesting that there appeared to be a slight kink in the passivation curve at potentials of approximately 500 mV, Figs. 4-6. This appeared to be particularly prevalent in the aqueous environments, Fig. 4-6. Whether this could be attributed to a change in the chemistry of the passivation process above such potentials will be addressed further below.

It should be noted that the results above indicated that the cathodic current densities increased as a function of velocity, and that this reaction was also reduced in the oil water conditions. However it was interesting that the cathodic currents in oil, Figs. 4(b), 5(b), 6(b), were significantly higher than the anodic currents, and that this difference was not pronounced in the water environments, Figs. 4-6.

3.2 Weight change data

The overall weight loss K_{ec} was recorded at potentials of 0 and 400 mV, Figs. 7-13.

The weight change during erosion-corrosion can be given as follows;

$$K_{ec} = K_{co} + K_{eo} + \Delta K_e + \Delta K_c \quad (1)$$

$$\text{where } K_e = K_{eo} + \Delta K_e \text{ and} \quad (2)$$

$$K_c = K_{co} + \Delta K_c \quad (3)$$

and K_{ec} is total erosion-corrosion rate, K_{eo} is the erosion rate in absence of corrosion, K_{co} is the corrosion rate in the absence of erosion, ΔK_e is the effect of corrosion on the erosion rate and ΔK_c is the effect of erosion on the corrosion rate. The individual contributions are given in Tables 1-6 at the various impact angles. The values of K_c were calculated from the Faradaic conversion of the corrosion current density to mass loss [12].

The results Figs. 7-9, at 0 mV, that there was an increase in erosion-corrosion rate with increasing velocity in all conditions studied. The value of K_c was highest in the reservoir water, Fig. 7 (where it exceeded that of K_e), and at a minimum in the crude oil, Fig. 8. In oil containing solutions, Figs. 8-9, the value of K_c was always less than K_e .

At 400 mV, Figs. 10-12, a largely similar pattern of behaviour was observed, with the lowest values of K_c observed in crude oil, Fig. 11. However, in the reservoir water, Fig. 10(a-b), at the lower impact angle range, there was little differences between the values of K_e and K_c , unlike the behaviour observed at the lower applied potentials, Fig. 7(a-b). It was interesting that at normal impact, Fig. 10 (c), the situation where K_c exceeded K_e again predominated. This indicates that applied potential and impact angle effects were significant in changing the erosion-corrosion regimes in such environments.

3.2 Microscopy analysis

Scanning electron micrographs, Fig. 13-14 indicated changes in surface morphology in the various environments. The surface at 0 mV and at 45° after impact at 3.5 ms^{-1} in water was relatively smooth, Fig. 13(a). More evidence of film formation was observed in oil, Fig. 13 (b) and in the oil/water environment, Fig. 13(c), and there was evidence of passive film amid some dispersed oil deposits on the surface. At higher impact velocities and potentials, i.e. 4.5 ms^{-1} at 90° and 400 mV, the surface formed in water, Fig. 14(a) was significantly rougher. A relatively smooth morphology, by contrast was observed in oil, Fig. 14(b), with clear evidence, in the oil water system, of an oxide film combined with oil deposits, Fig. 14(c).

4. Discussion

4.1 Trends on the observed erosion-corrosion behaviour in the various slurry environments

It is clear that the passivation rate in the presence of oil is reduced considerably compared to water only systems, Figs. 6-12, and that as passivation is indicated in all environments, the presence of the oil must have an effect on the passivation and re-passivation kinetics. Such trends have also been observed in a recent study on steels in similar conditions. The role of the adsorbed oil film is considered to increase the transport of oxygen to the surface and therefore to increase the cathode kinetics as oxygen has a higher solubility in oil than in water [2]. This increase in cathodic current density is observed particularly in the oil containing environments Figs. 4-6, as seen above. On the other hand, the anodic current density is reduced (attributed to the lower solubility of Fe ions in oil), and therefore passivation is considered less likely to occur and the values of K_c are very low in such conditions. Hence, the oil layer can have an important role in reducing erosion-corrosion in such environments.

In the water environments, Fig. 6-12, the effect of applied potential changes the dominance of the erosion and corrosion regimes compared to that observed in the other environments. For example, there is a consistent pattern in the water environment only, Fig. 7 at 0 mV of K_c exceeding K_e , with this trend decreasing at the higher potentials i.e. Fig. 10. This is attributed to the ability of the passive film to withstand particle impacts at such potentials- at higher potentials, with a marginally thicker film, the integrity of the film may be lower. In the environments containing oil, Figs. 8-9, and Figs. 11-12, the value of K_c is always lower than K_e , indicating the reduction in passive film formation in such cases. This means that although the values of K_c are lower in crude oil conditions, Figs. 8-9, and Figs. 11-12, the conditions where the passive film can withstand particle erosion may be less likely to be obtained in crude oil conditions and that optimizing the oil content must be carried out to ensure optimum erosion performance from the passive film in such conditions.

It is interesting that the current density increases when impact angle is increased from 15° to 45° but does not increase with further increases in impact angle from 45° to 90°, Fig. 4-6 and that this pattern is also affected by changes in potential and the chemistry of the environment. At low impact angles, the erosion of passive film material is likely to increase up to a critical impact angle and to remain constant or marginally decrease due to a decrease in cutting wear at higher impact angles and this is a possible reason for this observation [13-14].

4.2 Erosion-corrosion maps

Erosion-corrosion mechanism maps, Figs. 15-16, have been constructed based on the results at 0 and 400 mV, where erosion-corrosion regime transitions are presented as a function of velocity and impact angle and the various contributions are calculated, as outlined in Tables 1-6.

The regime transitions are as follows:

$K_e/K_c < 0.1$	Passivation-dominated	(4)
$1 > K_e/K_c \geq 0.1$	Passivation-erosion	(5)
$10 > K_e/K_c \geq 1$	Erosion-passivation	(6)
$K_e/K_c \geq 10$	Erosion-dominated	(7)

The maps indicate that not surprisingly the extent of passivation is at a maximum in water, Fig. 15(a), where passivation -erosion dominated the majority of the area of the map. It is at a minimum in oil, Fig. 15(b), where erosion-dominated behaviour prevails. In the oil/ water environment, the intermediate situation of erosion-passivation occurs over the parameter space studied. It is interesting that increases in velocity and impact angle increases the corrosion affected regimes, and this may be due to enhanced mass transfer of oxygen to the surface at the higher velocities and the reduction in erosion of the passive film at higher impact angles. Why the passive film may be less vulnerable at higher impact angles is difficult to ascertain but may be due to less likelihood of cutting wear at such impact angles [13-14].

At higher potentials, i.e. 400 mV, Fig. 16(a) similar observations to the above are made for the steel in the water environment. However in this case, the effect of increasing velocity is to initially increase the corrosion and then at higher velocities reduce it, consistent with the increase of mechanical energy into the system. At such potentials, the films appear, according to the map, to be more vulnerable to erosion than those formed at lower applied potentials. For the oil and water conditions the maps are identical to those observed at lower potentials, Fig. 16(b-c).

Erosion-corrosion wastage maps, Figs. 17-18, have been generated to demonstrate the transition between wastage regimes, where low, medium and high regimes are less or equal to $6 \text{ mg cm}^{-2} \text{ h}^{-1}$, between 6 and $50 \text{ mg cm}^{-2} \text{ h}^{-1}$, and greater or equal to $50 \text{ mg cm}^{-2} \text{ h}^{-1}$.

Clearly, the passive film has some effect in reducing the erosion-corrosion at low impact angles and velocities, in water, as shown in Fig. 17(a). However, the effect of the oil film is to considerably reduce the erosion-corrosion rate, Fig. 17(b). This effect is less evident in the oil water slurry, Fig. 17(c) and for all conditions at higher potentials, Fig. 18(a-c), indicating that there is a window of conditions where the erosion-corrosion performance may be optimized in oil containing conditions.

Erosion-corrosion additive-synergism maps can be constructed, Figs. 19-20.

Here, regimes of erosion-corrosion can be defined depending whether the erosion-corrosion is additive, synergistic or antagonistic as defined elsewhere [5-7, 15] and below i.e.

Here :

$$\Delta K_e / \Delta K_c < 0.1 \quad \text{Additive} \quad (8)$$

$$1 > \Delta K_e / \Delta K_c \geq 0.1 \quad \text{Additive-synergistic} \quad (9)$$

$$\Delta K_e / \Delta K_c > 1 \quad \text{Synergistic} \quad (10)$$

Additive behaviour defines the situation where the enhancement of corrosion due to erosion is greater than the effect of corrosion on the erosion.

Where corrosion may enhance the erosion, the interaction is defined as synergistic behaviour. Where it inhibits erosion i.e where the formation of surface film reduces erosion, then the reverse occurs and the mechanism is defined as antagonistic.

Both synergistic and antagonistic behaviour are characteristics of erosion-corrosion processes [5-7] and a method needs to be defined to illustrate such differences. If a film forms on the surface in the exposure conditions which is effective in reducing erosion, i.e. $\Delta K_e/\Delta K_c > -1$, then “synergistic” should be replaced by “antagonistic” for the above and the inequalities are negative as illustrated elsewhere [5-7].

The results, Fig. 19 at 0 mV, indicate that the additive regime, where erosion is enhancing corrosion i.e. through removal and reformation of passive film is highest in water, Fig. 19(a). In the oil and oil/water conditions, the antagonistic regime where the film is reducing wear, is observed to much greater extent. Regimes of antagonism and synergism sit in different envelopes of conditions in the oil and oil/water slurries, Figs. 19(b-c), possibly indicating different mechanisms of protecting the surfaces in such cases. At higher potentials, different regime transitions are observed, with the level of additive behaviour now reduced in the water conditions, Fig. 20(a). The level of antagonistic behaviour reduces in the oil conditions but increases in the oil/water conditions, Figs. 20(b-c), indicating that the passivation chemistry may have a significant effect on the ability of the surface to provide protection against erosion-corrosion in such conditions.

Clearly, such maps may provide important insights into the change of mechanism of erosion-corrosion in such conditions and recent work has been focused on the development of such diagrams for micro-abrasion-corrosion of materials [16]. Further work will be to investigate the change of regime boundaries in a wider range of conditions in addition to evaluating whether such observations may be observed for other materials such as surface coatings [17] and different tribological conditions in such environments.

5. Conclusions

- (i) Effects of velocity and impact angle have been evaluated for the erosion-corrosion of carbon steel in a range of aqueous/crude oil slurries.
- (ii) The results indicate that oil containing environments may provide resistance to erosion depending on the conditions
- (iii) Erosion-corrosion maps have been constructed showing the change in erosion-corrosion mechanisms, the levels of wastage and extent of synergistic/antagonistic behavior based on the results.



Fig. 1: Example of erosion-corrosion degradation of piping in downstream oil production condition.



Fig. 2: Example of erosion-corrosion of a joint at upstream oil production.

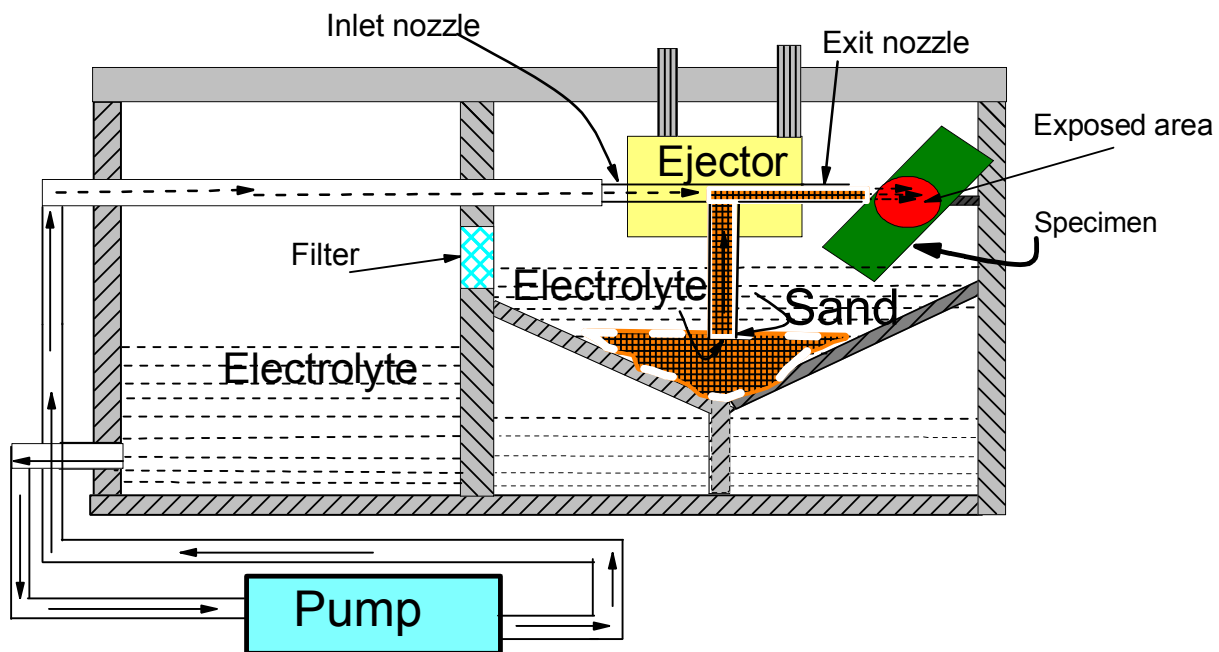


Figure (3) Schematic diagram of erosion-corrosion test rig.

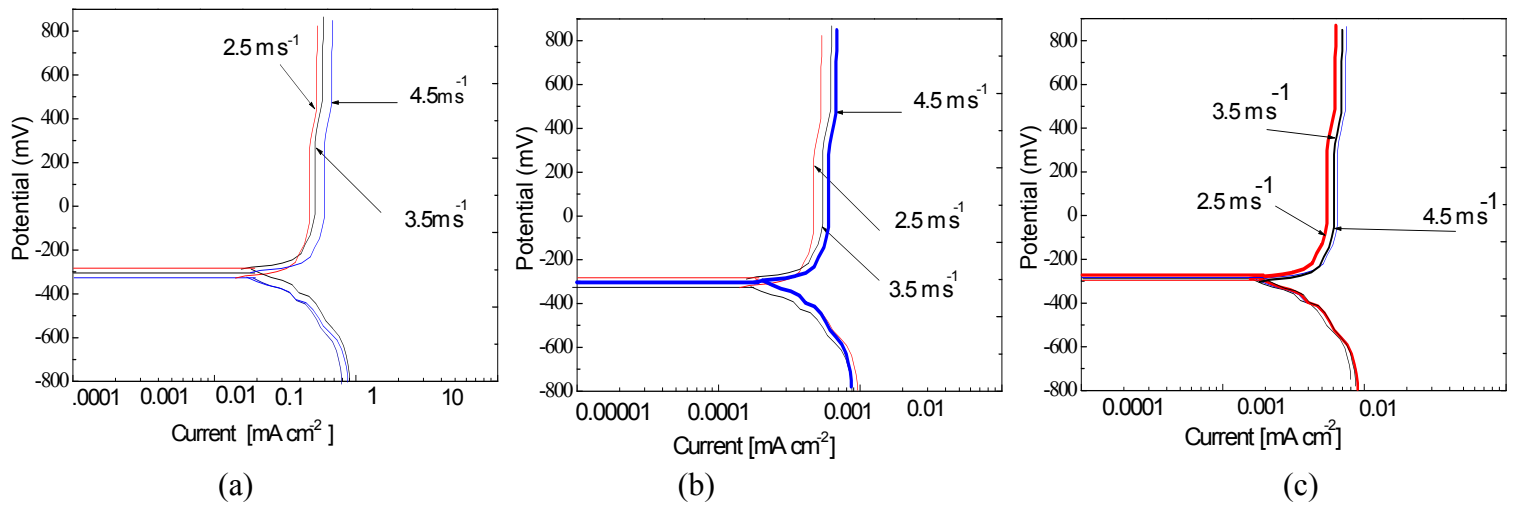


Fig (4): Polarization curves for carbon steel at various impact velocities, at impact angle 15° in (a) water (b) crude oil (c) 20% water/crude oil.

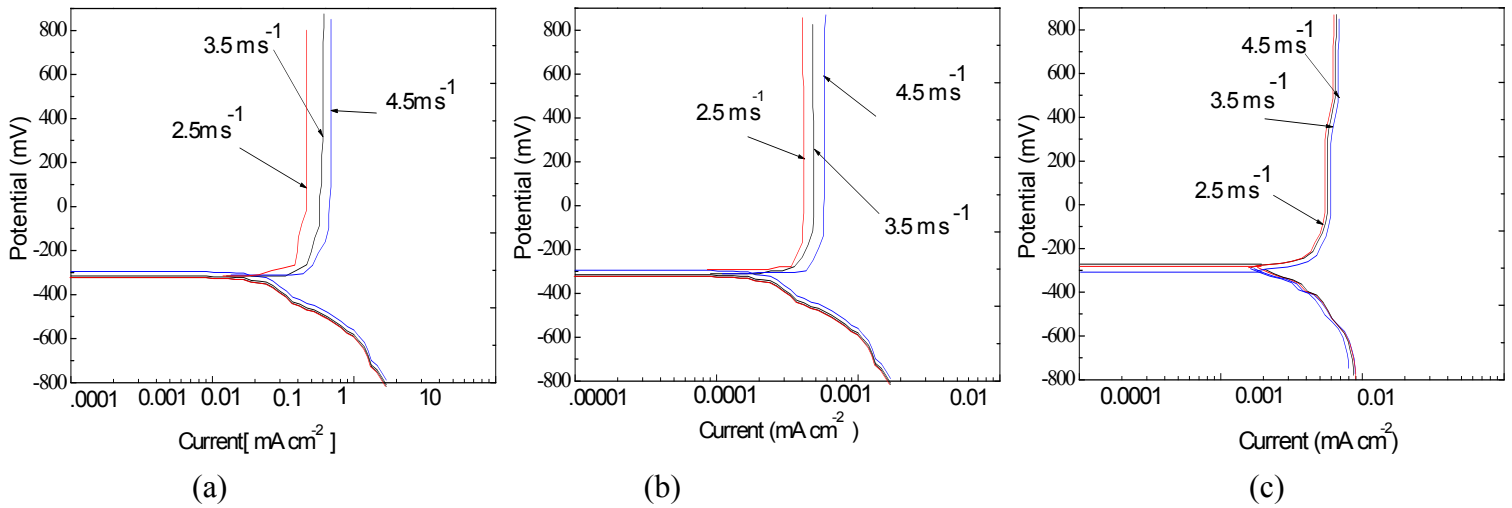


Fig (5): Polarization curves for carbon steel at various impact velocities, at impact angle 45° in (a) water (b) crude oil (c) 20% water/crude oil.

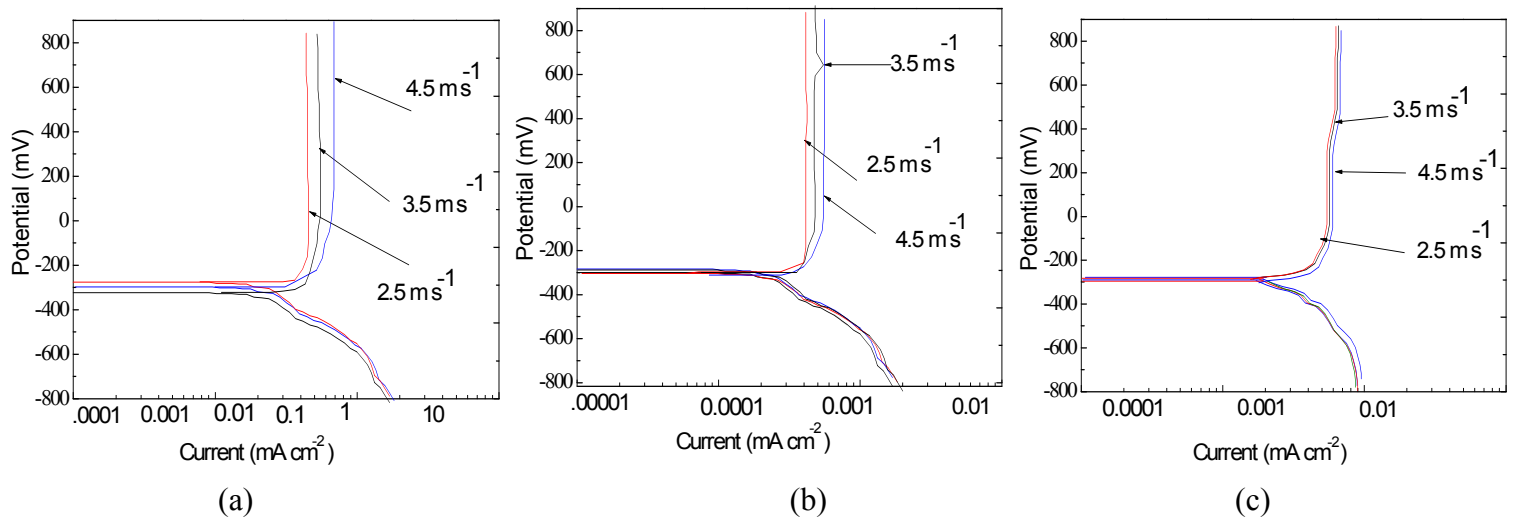


Fig (6): Polarization curves for carbon steel at various impact velocities, at impact angle 90° in (a) water (b) crude oil (c) 20% water/ crude oil.

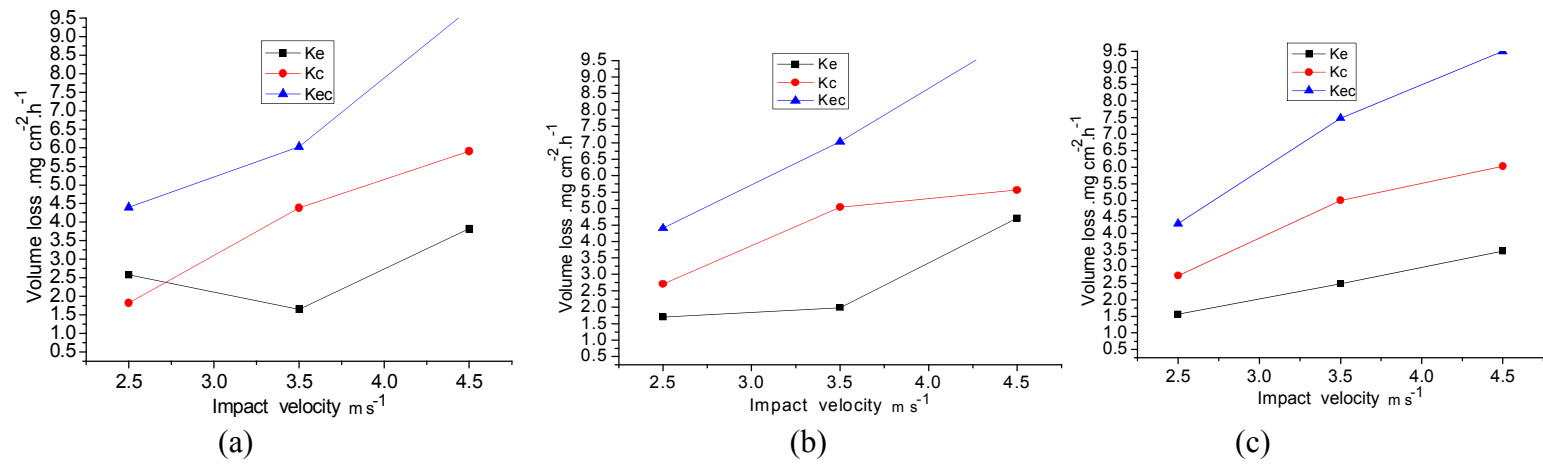


Fig (7): Volume loss as function of impact velocity for carbon steel in water at 0 mV (a) 15° (b) 45° (c) 90°.

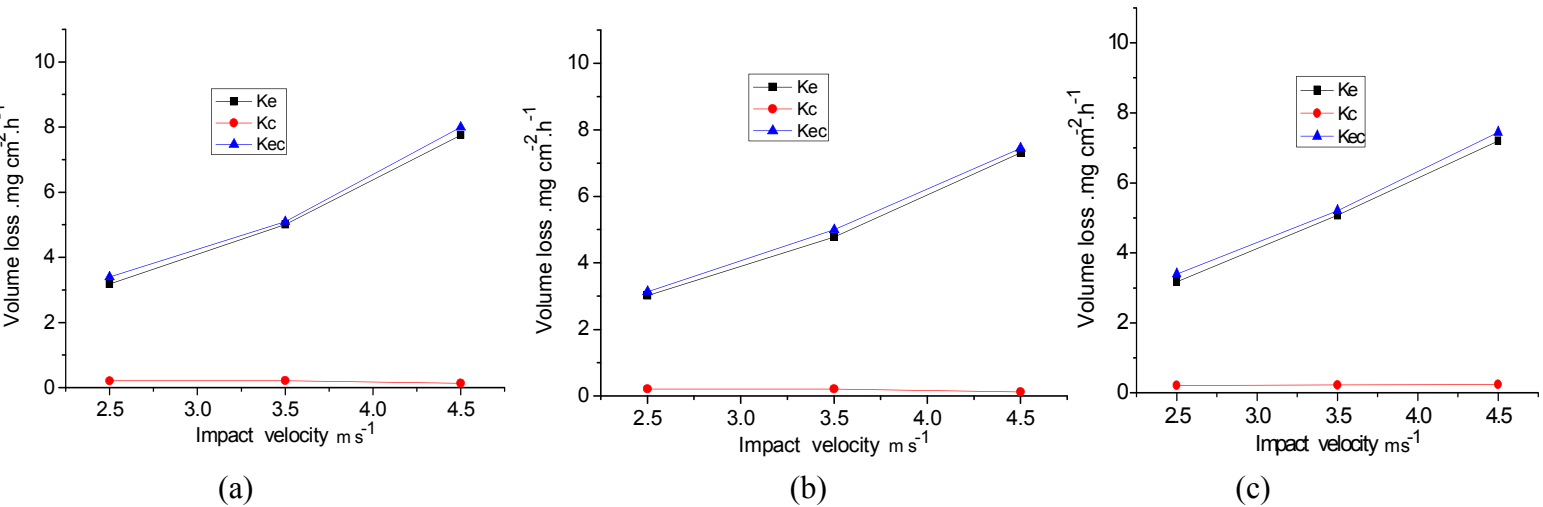


Fig (8): Volume loss as function of impact velocity for carbon steel in crude oil at 0 mV (a) 15° (b) 45° (c) 90°.

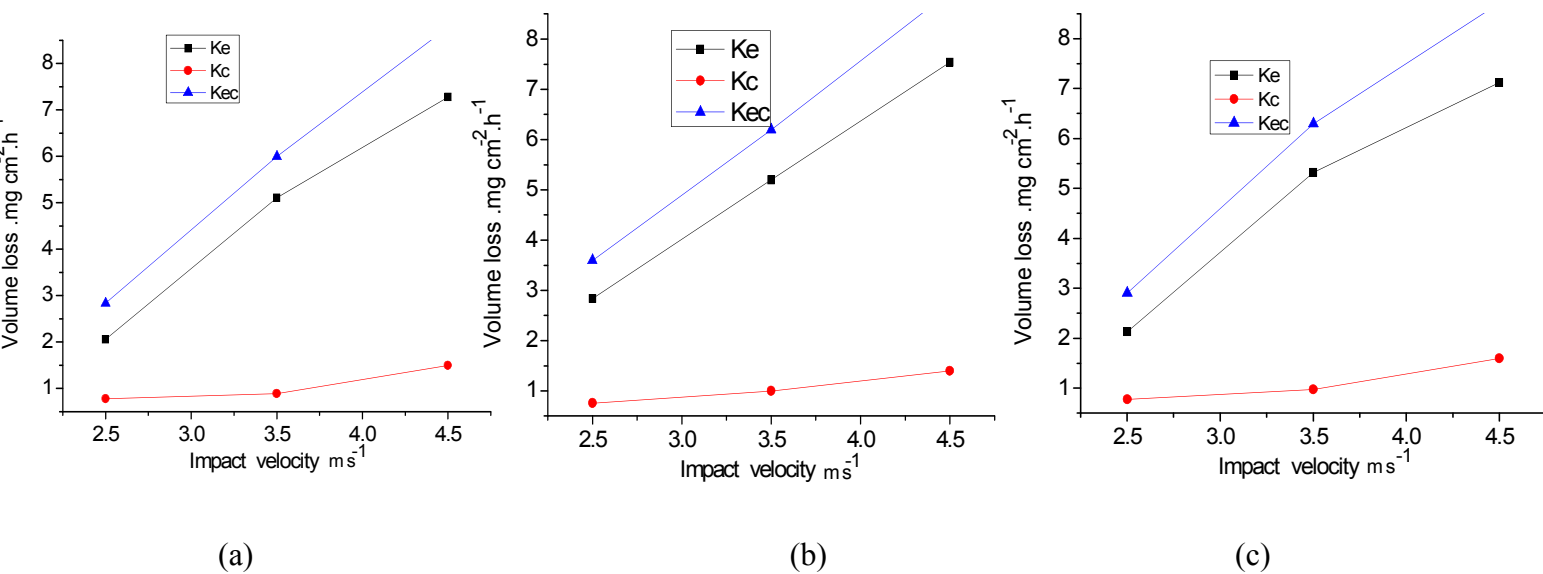


Fig (9): Volume loss as function of impact velocity for carbon steel in 20% water/crude oil at 0 mV (a) 15° (b) 45° (c) 90°.

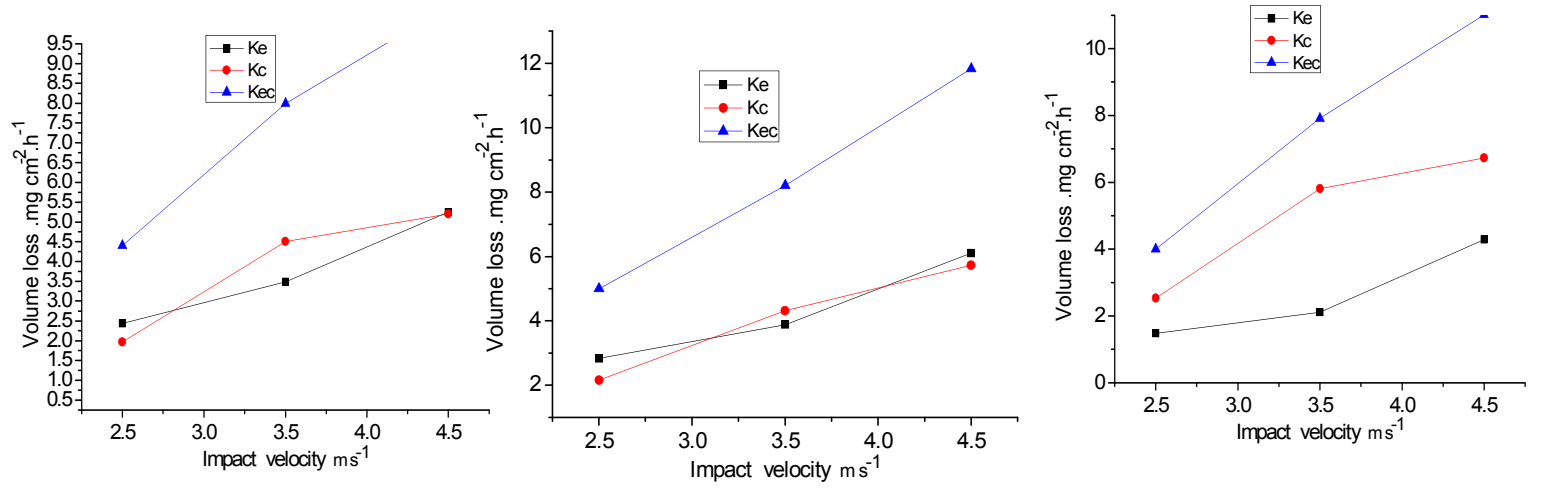


Fig (10): Volume loss as function of impact velocity for carbon steel in water at 400 mV (a) 15° (b) 45° (c) 90°.

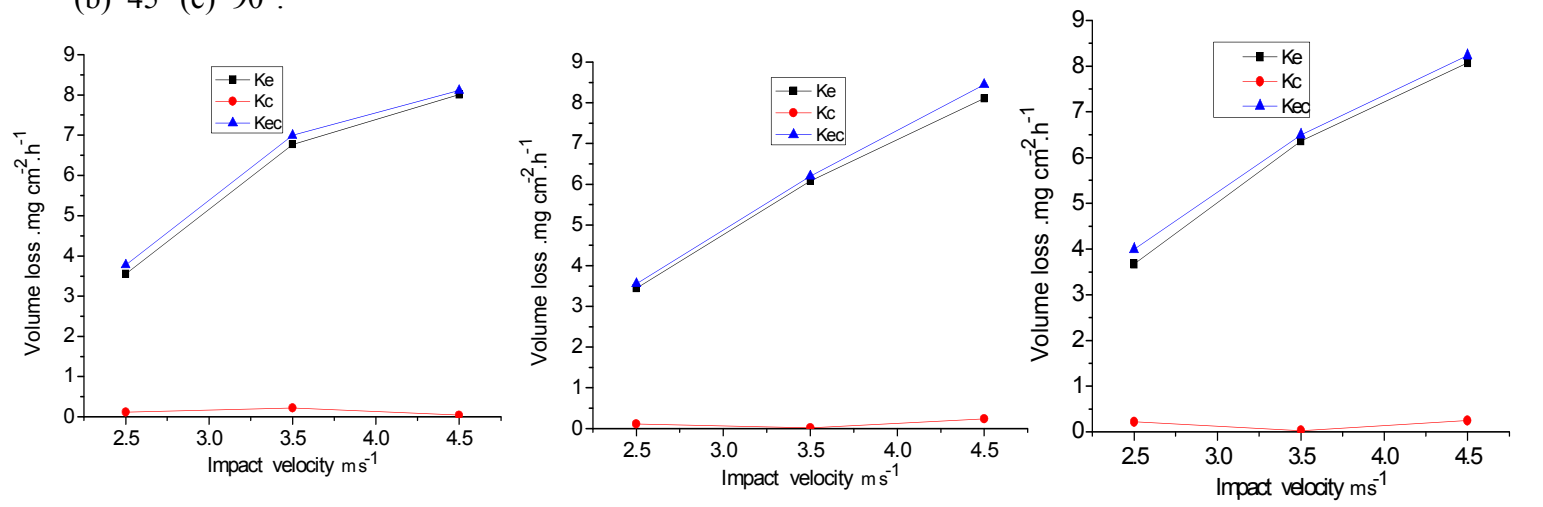


Fig (11): Volume loss as function of impact velocity for carbon steel in crude oil at 400 mV (a) 15° (b) 45° (c) 90°.

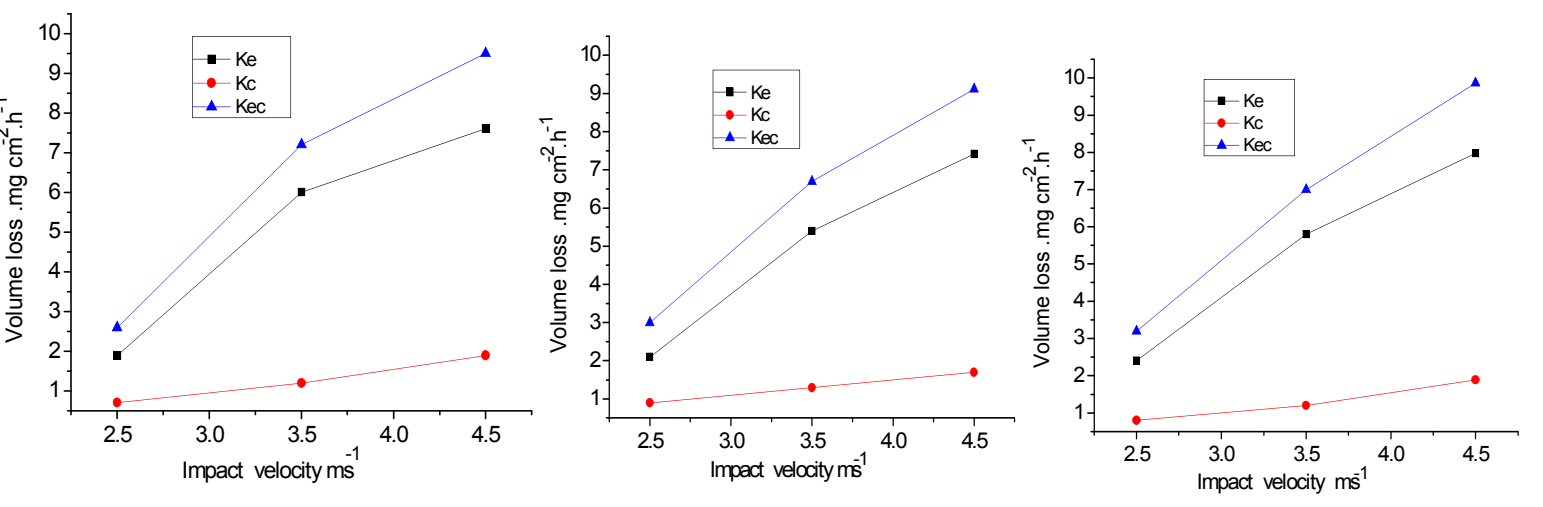


Fig (12): Volume loss as function of impact velocity for carbon steel in 20% water/ crude oil at 400 mV (a) 15° (b) 45° (c) 90°.

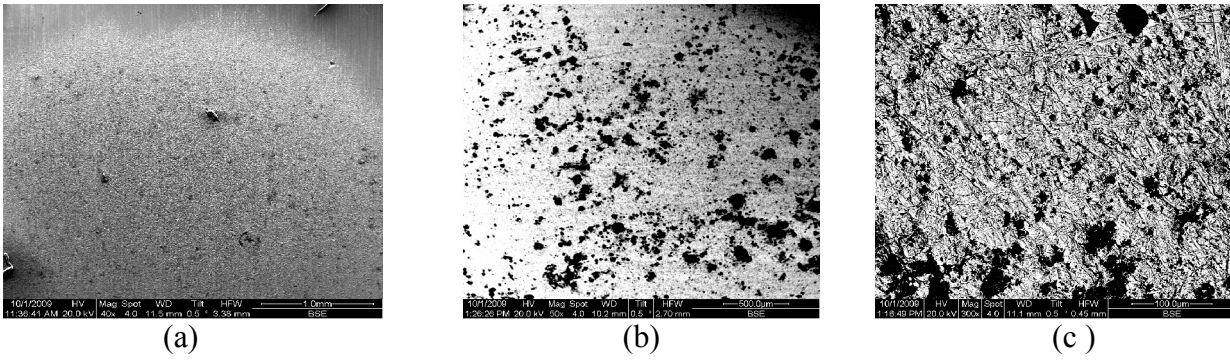


Fig (13): Scanning electron micrographs of eroded carbon steel test specimen at $V=3.5 \text{ m s}^{-1}$, 0 mV and impact angle 45° :(a)in water (b) in crude oil (c)in 20% water/ crude oil.

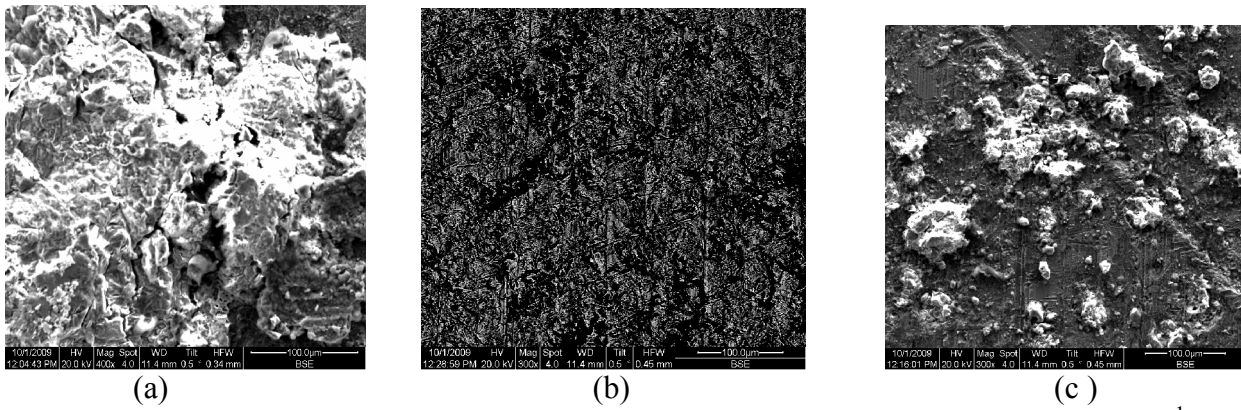
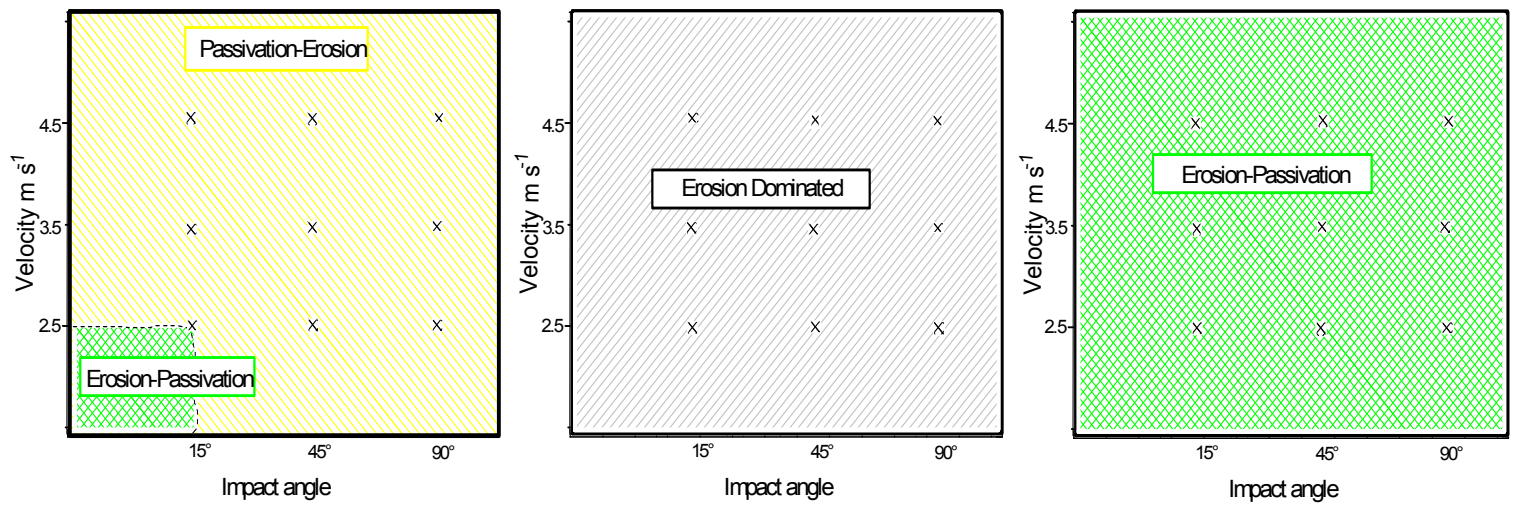
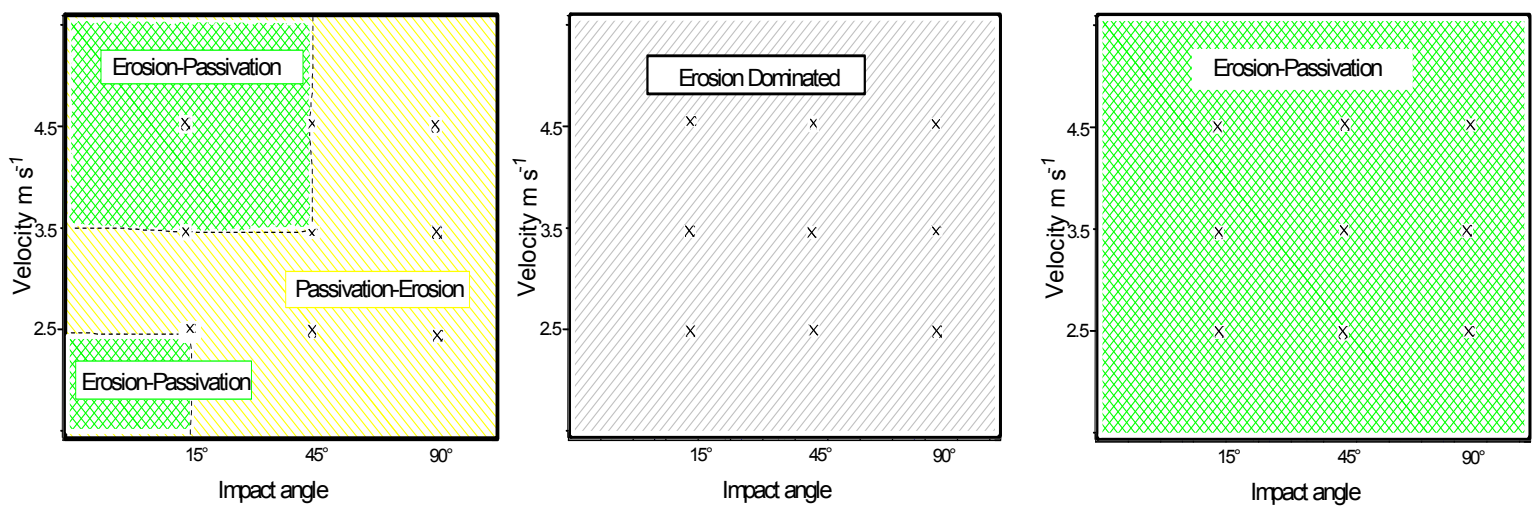


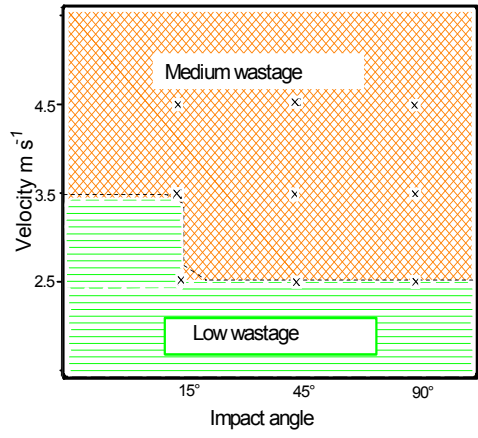
Fig (14): Scanning electron micrographs of eroded carbon steel test specimen at $V=4.5 \text{ m s}^{-1}$, 400 mV and impact angle 90° :(a)in water (b) in crude oil (c)in 20% water/ crude oil.



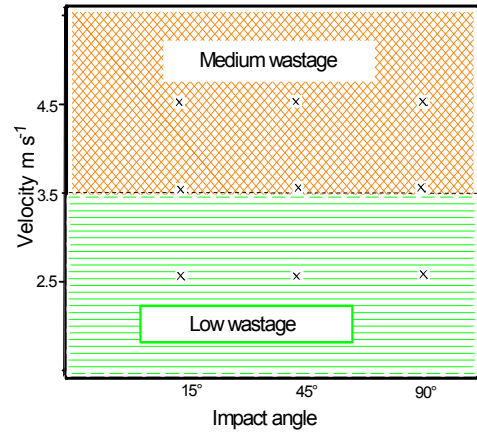
(a) (b) (c)
 Fig (15): Erosion-Corrosion mechanism maps for carbon steel at 0 mV in (a) water (b) crude oil (c) 20% water/ crude oil.



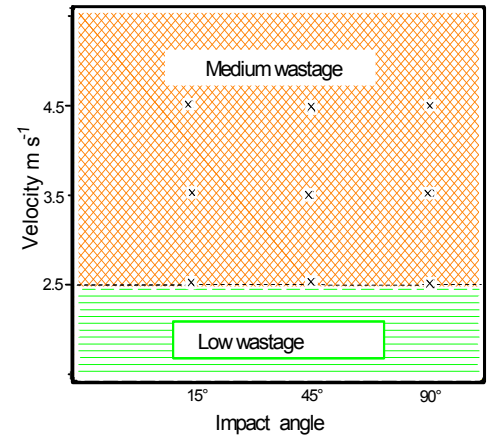
(a) (b) (c)
 Fig (16): Erosion-Corrosion mechanism maps for carbon steel at 400 mV in (a) water (b) crude oil (c) 20% water/ crude oil.



(a)

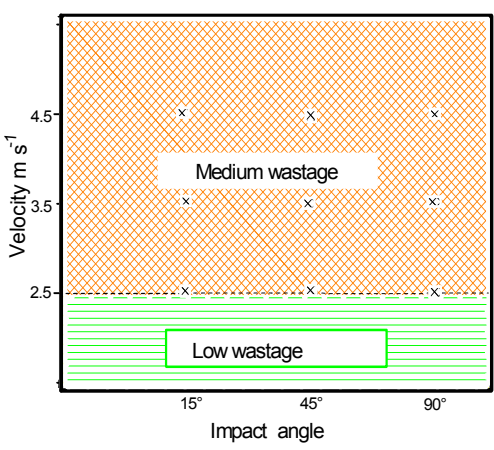


(b)

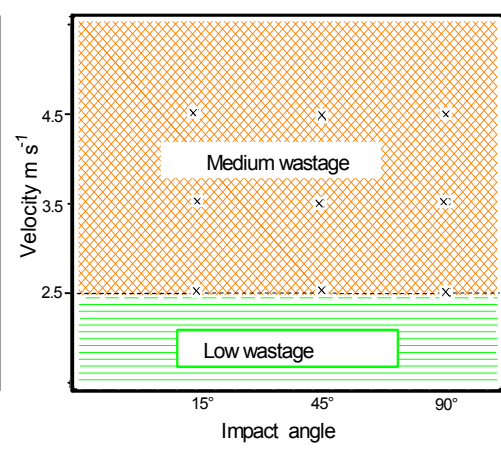


(c)

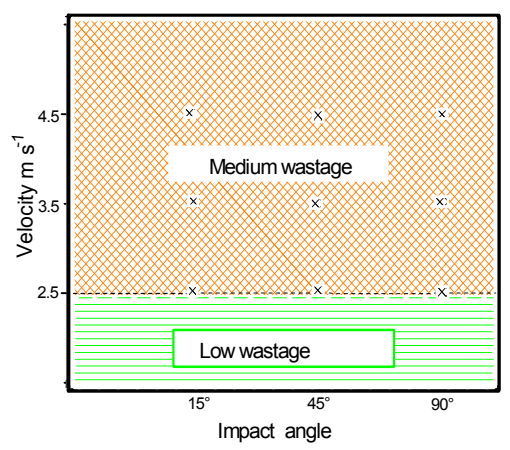
Fig (17): Erosion-corrosion wastage maps for carbon steel at 0 mV in (a) water (b) crude oil (c) 20% water/ crude oil.



(a)

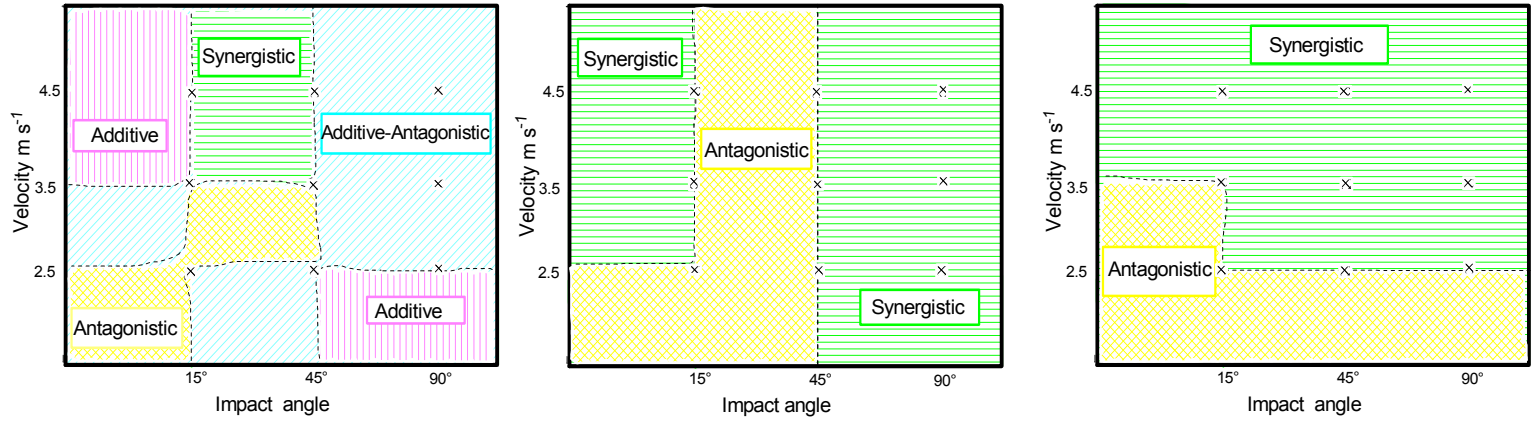


(b)

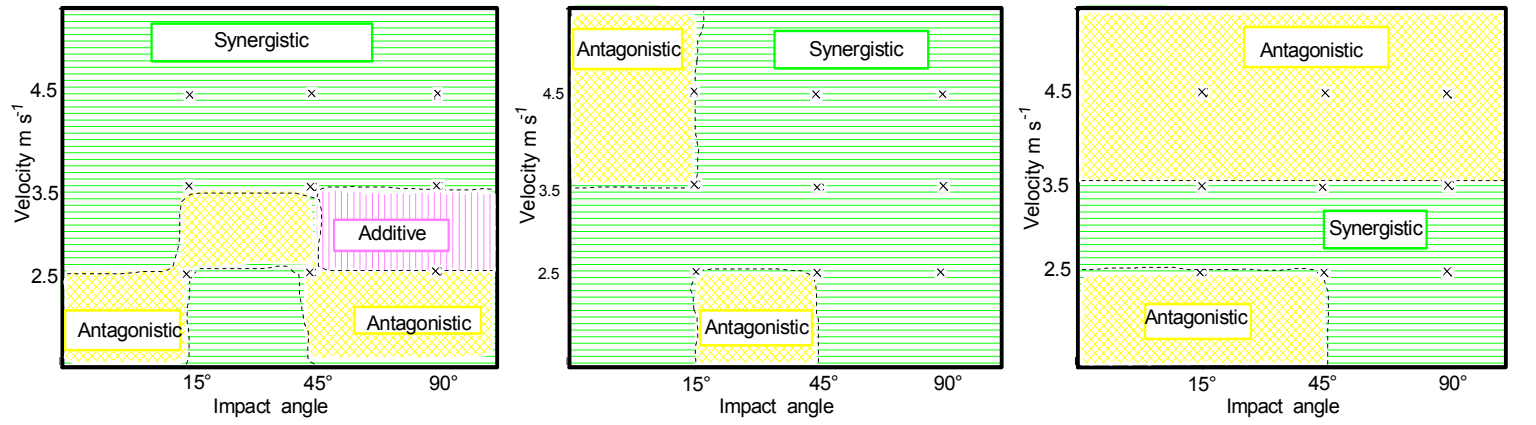


(c)

Fig (18): Erosion-corrosion wastage maps for carbon steel at 400 mV in (a) water (b) crude oil (c) 20% water/ crude oil.



(a) (b) (c)
 Fig (19): Erosion-corrosion additive-synergism maps for carbon steel at 0 mV in (a) water (b) crude oil (c) 20% water/ crude oil.



(a) (b) (c)
 Fig (20): Erosion-corrosion additive-synergism maps for carbon steel at 400 mV in (a) water (b) crude oil (c) 20% water/ crude oil.

Tables

Table 1: Volume loss as a function of impact velocity and impact angle for carbon steel in water at 0 mV
(a) 15°

velocities m s^{-1}	Ke	Kc	Δke	Δkc	$\Delta ke/\Delta kc$	Ke/Kc	Kec
2.5	2.6	1.8	0.9	-0.2	-5.5	1.4	4.4
3.5	1.7	4.4	-0.4	0.9	-0.4	0.4	6.0
4.5	3.8	5.9	0.8	1.1	0.8	0.7	9.7

(b) 45°

velocities m s^{-1}	Ke	Kc	Δke	Δkc	$\Delta ke/\Delta kc$	Ke/Kc	Kec
2.5	1.7	2.71	-0.8	1.5	-0.5	0.6	4.4
3.5	2	5.0	-1.2	0.2	-5.3	0.4	7
4.5	4.7	5.6	1.6	0.3	6.4	0.9	10

(c) 90°

velocities m s^{-1}	Ke	Kc	Δke	Δkc	$\Delta ke/\Delta kc$	Ke/Kc	Kec
2.5	1.6	2.7	-0.03	0.5	-0.1	0.6	4.3
3.5	2.5	5	0.3	1	0.3	0.5	7.48
4.5	3.5	6	0.6	0.8	0.7	0.6	9.5

Table 2: Volume loss as a function of impact velocity and impact angle for carbon steel in water at 400 mV
(a) 15°

velocities m s^{-1}	Ke	Kc	Δke	Δkc	$\Delta ke/\Delta kc$	Ke/Kc	Kec
2.5	2.4	2	0.7	-0.1	-10.6	1.24	4.41
3.5	3.5	4.5	1.5	0.5	3	0.8	8
4.5	5.3	5	2.3	0.1	19	1.0	10.3

(b) 45°

velocities m s^{-1}	Ke	Kc	Δke	Δkc	$\Delta ke/\Delta kc$	Ke/Kc	Kec
2.5	2.8	2.2	0.3	0.3	1.1	1.3	5
3.5	3.9	4.3	0.7	-0.5	-1.4	0.9	8.2
4.5	6.1	5.7	2.2	0.8	2.6	1.1	11.8

(c) 90°

velocities m s^{-1}	Ke	Kc	Δke	Δkc	$\Delta ke/\Delta kc$	Ke/Kc	Kec
2.5	1.5	2.5	-0.1	0.1	-1.2	0.6	4.0
3.5	2.1	5.8	-0.1	1.5	-0.1	0.4	7.9
4.5	4.3	6.7	1.4	1.0	1.4	0.6	11.0

Tables 3: Volume loss as a function of impact velocity and impact angle for carbon steel in crude oil at 0 mV
(a) 15°

velocities $m s^{-1}$	Ke	Kc	Δke	Δkc	$\Delta ke/\Delta kc$	Ke/Kc	Kec
2.5	3.4	0.0185	1.403	-0.0006	-2338	183	3.401
3.5	5.1	0.0259	2.774	0.0058	478	196	5.1
4.5	7.95	0.0428	4.357	0.0018	2421	186	8

(b) 45°

velocities $m s^{-1}$	Ke	Kc	Δke	Δkc	$\Delta ke/\Delta kc$	Ke/Kc	Kec
2.5	3.13E+00	0.0139	1.226	-0.0006	-2044	225	3.14
3.5	5	0.0181	2.6	-0.0011	-2347	275	5
4.5	7	0.0308	4.2	-0.0046	-917	241	7.5

(c) 90°

velocities $m s^{-1}$	Ke	Kc	Δke	Δkc	$\Delta ke/\Delta kc$	Ke/Kc	Kec
2.5	3.38E+00	0.02	1.7	0.0005	3360	169	3.4
3.5	5	0.0291	3.1	0.0069	453	178	5.21
4.5	7	0.0456	4.2	0.0104	404	162	7.45

4: Volume loss as a function of impact velocity and impact angle for carbon steel in crude oil at 400 mV
(a) 15°

velocities $m s^{-1}$	Ke	Kc	Δke	Δkc	$\Delta ke/\Delta kc$	Ke/Kc	Kec
2.5	3.8	0.0214	1.8	0.0029	613	176	3.78
3.5	7	0.0258	4.7	0.00051	9348	270	7
4.5	8	0.0478	4.5	-0.0002	-22361	169	8.12

(b) 45°

velocities $m s^{-1}$	Ke	Kc	Δke	Δkc	$\Delta ke/\Delta kc$	Ke/Kc	Kec
2.5	3.6	0.014	1.645	-0.0013	-1266	283	3.56
3.5	6	0.0202	3.77	0.0005	7559	356	6.2
4.5	8	0.04	5.21	0.0008	6512	210	8.45

(c) 90°

velocities $m s^{-1}$	Ke	Kc	Δke	Δkc	$\Delta ke/\Delta kc$	Ke/Kc	Kec
2.5	4	0.0265	2.274	0.007	324.79	154.094	4.11
3.5	6	0.0321	4.417	0.0078	566	201	6.5
4.5	8	0.0518	4.97	0.0101	492	157	8.23

Table 5: Volume loss as a function of impact velocity and impact angle for carbon steel in 20 % water/crude oil at 0 mV.

(a) 15°

velocities m s ⁻¹	Ke	Kc	Δke	Δkc	Δke/Δkc	Ke/Kc	Kec
2.5	2.1	0.8	0.1	-0.08	-1	2.6	2.8
3.5	5.1	0.9	2.8	-0.03	-93.7	5.7	6
4.5	7.3	1.5	3.7	0.2	18	4.9	8.8

(b) 45°

velocities m s ⁻¹	Ke	Kc	Δke	Δkc	Δke/Δkc	Ke/Kc	Kec
2.5	2.8	0.8	0.9	-0.04	-23.5	3.7	3.6
3.5	5.2	1	2.8	0.1	28	5.2	6.2
4.5	7.5	1.4	4.3	0.2	21.7	5.4	8.9

(c) 90°

velocities m s ⁻¹	Ke	Kc	Δke	Δkc	Δke/Δkc	Ke/Kc	Kec
2.5	2.1	0.8	0.43	-0.02	-21.5	2.7	2.91
3.5	5.3	1	3.3	0.2	16.4	5.4	6.3
4.5	7.1	1.6	3.9	0.3	13.1	4.5	8.72

Table 6: Volume loss as a function of impact velocity and impact angle for carbon steel in 20% water/crude oil at 400 mV

(a) 15°

velocities m s ⁻¹	Ke	Kc	Δke	Δkc	Δke/Δkc	Ke/Kc	Kec
2.5	1.9	0.7	-0.1	-0.1	1	2.7	2.6
3.5	6.0	1.2	3.7	0.2	18.6	5	7.2
4.5	7.6	1.9	4.01	-0.1	-40	4	9.5

(b) 45°

velocities m s ⁻¹	Ke	Kc	Δke	Δkc	Δke/Δkc	Ke/Kc	Kec
2.5	2.1	0.9	0.2	0.2	1	2.	3
3.5	5.4	1.3	3	0.5	6.5	4.2	6.7
4.5	7.4	1.7	4.2	-0.1	-52.6	4.4	9.12

(c) 90°

velocities m s ⁻¹	Ke	Kc	Δke	Δkc	Δke/Δkc	Ke/Kc	Kec
2.5	2.4	0.8	0.7	0.02	35	3	3.2
3.5	5.8	1.2	3.8	0.4	10.42	4.8	7
4.5	8	1.9	4.8	-0.11	-43.5	4.2	9.87

References

- [1] Hamzah R, Stephenson, D.J. and Strutt J.S. (1995) "Erosion of material used in petroleum production" *Wear*, 186-187, pp.493-496.
- [2] Tian, B.R. and Cheng, Y.F. (2008) "Electrochemical corrosion behavior of X-65 steel in the simulated oil sand slurry. I. Effects of hydrodynamic condition" *Corrosion Science* 50, pp.773-779.
- [3] Fang Yu, Xiaolu Pang and Guoan Zhang (2008) "Mechanical properties of CO₂ corrosion product scales and their relationship to corrosion rates" *Corrosion Science* 50, pp.2796–2803.
- [4] Stack, M.M. and Pungwiwat N, (2004), "Erosion–corrosion mapping of Fe in aqueous slurries: some views on a new rationale for defining the erosion–corrosion interaction", *Wear*, 256, 5, pp. 565-576.
- [5] Stack, M.M. and Abd El Badia, T.M. (2006) Mapping erosion–corrosion of WC/Co–Cr based composite coatings: particle velocity and applied potential effects. *Surf. Coat. Technol.* 201, pp.1335-1347.
- [6] Stack, M.M. and Abd El Badia, T.M. (2006) "On the construction of erosion–corrosion maps for WC/Co–Cr based coatings in aqueous conditions" *Wear* 261, pp.1181-1190.
- [7] Stack, M.M. and Abd El Badia, T.M. (2008), "Some comments on mapping the combined effects of slurry concentration, impact velocity and electrochemical potential on the erosion–corrosion of WC/Co–Cr coatings" *Wear*, 264, 9-10, pp. 826-837.
- [8] Neville, A., Hodgkiess, T. and Dallas, J.T. (1995) "A study of the erosion-corrosion behaviour of engineering steels for marine pumping applications". *Wear* 186-187, pp.497-507.
- [9] Wood, R.J.K (2006), "Erosion–corrosion interactions and their effect on marine and offshore materials", *Wear*, 261, 9, pp. 1012-1023.
- [10] Burstein, G.T, Li, Y. and Hutchings, I.M. (1995) "The influence of corrosion on the erosion of aluminium by aqueous silica slurries." *Wear*, 186-187, pp.515-522.
- [11] Zu, J. B. and Hutchings, I. M. and Burstein, G. T. (1990) "Design of a slurry erosion test rig" *Wear*, 140 (2). pp. 331-344.

- [12] ASTM Standard G 102, Standard Practice for Calculation of Corrosion Rates, ASTM, 1916 Race St., Philadelphia, Pennsylvania 19013-1187 (USA).
- [13] Finnie I, Wolak J and Kabil Y, “Erosion of Metals by Solid Particles” (1967) *J Mater*, 2, pp. 682-700.
- [14] Cousens AK and Hutchings I M (1981), Proc. 6th Int Conf on Erosion by Liquid and Solid Impact”, Cavendish Laboratory, University of Cambridge, paper 83.
- [15] ASTM G119 - 09 Standard Guide for Determining Synergism Between Wear and Corrosion, DOI: 10.1520/G0119-09.
- [16] Mathew, M.T. ,Stack, M.M, Matijevic B, Rocha, L.A. Ariza, E, (2008), “Micro-abrasion resistance of thermochemically treated steels in aqueous solutions: Mechanisms, maps, materials selection”, *Tribology International*, 41, 2, pp. 141-149.
- [17] Purandare, Y.P, Ehiasarian, A.P, Stack, M.M, Hovsepian, P.Eh (2010), “CrN/NbN coatings deposited by HIPIMS: A preliminary study of erosion–corrosion performance”, *Surface and Coatings Technology*, 204, 8, pp.1158-1162.